Synthesis of Organic Monolayer-Stabilized Copper Nanocrystals in Supercritical Water

Kirk J. Ziegler, R. Christopher Doty, Keith P. Johnston,* and Brian A. Korgel*

Contribution from the Department of Chemical Engineering, Texas Materials Institute and Center for Nano- and Molecular Science and Technology, The University of Texas at Austin, Austin, Texas 78712-1062

Received March 29, 2001

Abstract: When water is heated and pressurized above the critical point, it becomes a suitable solvent to employ organic capping ligands to control and stabilize the synthesis of nanocrystals. Without alkanethiol ligands, $Cu(NO_3)_2$ hydrolyzes to form polydisperse copper(II) oxide particles with diameters from 10 to 35 nm. However, in the presence of 1-hexanethiol, X-ray photoelectron spectroscopy, selected area electron diffraction, and transmission electron microscopy reveal the formation of copper nanocrystals ∼7 nm in diameter. The use of a different precursor, $Cu(CH_3COO)_2$, leads to particles with significantly different morphologies. A mechanism is proposed for sterically stabilized nanocrystal growth in supercritical water that describes competing pathways of hydrolysis to large oxidized copper particles versus ligand exchange and arrested growth by thiols to produce small monodisperse Cu nanoparticles.

Introduction

At the nanometer-length scale, material dimensions lead to quantum confinement effects that give rise to unique electronic and optical properties useful for a variety of new technologies including, electronic, optical, medical, coatings, catalytic, memory, and sensor applications.[1] A variety of wet chemical methods have been developed for nanocrystal synthesis. The main issues are control over particle size and size distribution, surface passivation, and core crystallinity. Metal nanocrystals, such as silver and gold, can be synthesized at room temperature;[2,3] whereas, semiconductor nanocrystals, such as CdSe[4] and InAs,[5] must be grown at high temperatures in high boiling point solvents to achieve crystalline cores and well-defined shape. The key ingredient in all of these methods is the use of capping ligands that bind to particle surfaces and provide a steric barrier to aggregation. The capping ligands tend to exhibit the properties of surfactants: one end binds strongly to the particle surface while the opposite end interacts with the solvating fluid. In a good solvent, the ligands extend from the nanocrystal surface and provide steric stabilization, which typically limits size to the nanometer range and prevents unwanted agglomeration.

Supercritical fluids (SCFs) offer several processing advantages over conventional solvents, which has led to increased use in materials chemistry[6−9] and more specifically, nanocrystal synthesis.[8−16] Supercritical CO_2 and supercritical water (SCW), for example, are chemically stable and environmentally benign. SCFs exhibit the combined characteristics of both gas and liquid solvents to provide a medium with densities characteristic of liquids and gaslike viscosities and diffusivities. Thus, mass-transfer rates approach those in gases, while solvation properties resemble those of conventional liquid solvents. Furthermore, supercritical fluids exhibit unique *tunable* solvation characteristics, as subtle changes in pressure and temperature in SCFs alter the solvent density. This property might be utilized to improve many aspects of nanocrystal processing—such as size-selective separations, synthesis, and self-assembly.

In water, the dielectric constant dramatically decreases ($\epsilon \approx 5$) when heated and pressurized above the critical point ($T_c = 374$ °C, $P_c = 221$ bar), which decreases the solubility of salts and increases the solubility of organics.[17] In certain applications, such as the supercritical water oxidation of organic wastes, the precipitation of salt particles is undesirable because it leads to reactor plugging and corrosion problems.[17,18] Recent efforts, however, have been made to control particle formation in SCW to create useful materials such as ceramics, coatings, and catalysts, with a variety of particulate chemistries being produced by hydrolyzing metal nitrates or metal acetates in

* Corresponding authors. For K.P.J.: (phone) (512) 471-4617; (fax) (512) 475-7824; (e-mail) kpj@che.utexas.edu. For B.A.K.: (phone) (512) 471-5633; (fax) (512) 471-7060; (e-mail) korgel@che.utexas.edu.

(1) Alivisatos, A. P. *Science* **1996**, *271*, 933−937.
(2) Brust, M.; Walker, M.; Bethell, D.; Schiffrin, D. J.; Whyman, R. *J. Chem. Soc., Chem. Commun.* **1994**, 801−802.
(3) Leff, D. V.; Ohara, P. C.; Heath, J. R.; Gelbart, W. M. *J. Phys. Chem.* **1995**, *99*, 7036−7041.
(4) Murray, C. B.; Norris, D. J.; Bawendi, M. G. *J. Am. Chem. Soc.* **1993**, *115*, 8706−8715.
(5) Banin, U.; Lee, C. J.; Guzelian, A. A., G.; Kadavanich, A. V.; Alivisatos, A. P.; Jaskolski, W.; Bryant, G. W.; Efros, A. L.; Rosen, M. *J. Chem. Phys.* **1998**, *109*, 2306−2309.
(6) Gogotsi, Y. G.; Yoshimura, M. *Nature* **1994**, *367*, 628−630.
(7) Watkins, J. J.; Blackburn, J. M.; McCarthy, T. J. *Chem. Mater.* **1999**, *11*, 213−215.
(8) Darr, J. A.; Poliakoff, M. *Chem. Rev.* **1999**, *99*, 495−541.
(9) Savage, P. E.; Gopalan, S.; Mizan, T. I.; Martino, C. J.; Brock, E. E. *AIChE J.* **1995**, *41*, 1723−1778.
(10) Holmes, J. D.; Bhargava, P. A.; Korgel, B. A.; Johnston, K. P. *Langmuir* **1999**, *15*, 6613−6615.
(11) Holmes, J. D.; Ziegler, K. J.; Doty, R. C.; Pell, L. E.; Johnston, K. P.; Korgel, B. A. *J. Am. Chem. Soc.* **2001**, *123*, 3743−3748.
(12) Holmes, J. D.; Johnston, K. P.; Doty, R. C.; Korgel, B. A. *Science* **2000**, *287*, 1471−1473.
(13) Cabanas, A.; Darr, J. A.; Lester, E.; Poliakoff, M. *Chem. Commun.* **2000**, 901−902.
(14) Cabanas, A.; Darr, J. A.; Lester, E.; Poliakoff, M. *J. Mater. Chem.* **2001**, *11*, 561−568.
(15) Galkin, A. A.; Kostyuk, B. G.; Lunin, V. V.; Poliakoff, M. *Angew. Chem., Int. Ed.* **2000**, *39*, 2738−2740.
(16) Galkin, A. A.; Kostyuk, B. G.; Kuznetsova, N. N.; Turakulova, A. O.; Lunin, V. V.; Polyakov, M. (sic) *Kinet. Catal.* **2001**, *42*, 154−162.
(17) Gloyna, E. F.; Li, L. *Waste Manage.* **1993**, *13*, 379−394.
(18) Kritzer, P.; Boukis, N.; Dinjus, E. *J. Supercrit. Fluids* **1999**, *15*, 205−227.

10.1021/ja010824w CCC: $20.00
Published on Web 07/20/2001

subcritical[13,14,19] or supercritical water.[8,15,16,20,21] For example, metal oxides have been prepared in SCW using metal nitrate salts, which decompose via a two-step mechanism of hydrolysis and dehydration.[20−23] The high temperature of SCW promotes crystallization, which eliminates the need for postprocess annealing. Different particle sizes and morphologies have been obtained with changes in reaction time, temperature, and pressure.[22,24−29] Additionally, the nature of the anion can affect the oxidation state of the metal, possibly as a result of oxidative mechanisms involving decomposition products of the precursor.[22] These results suggest that oxidants/reductants can be added to the reaction mixture to influence the product chemistry, as has been recently shown by the addition of oxalic acid to copper hydroxycarbonate.[16] Nanometer particle size control (i.e., <10-nm diameters), however, is difficult to achieve under these conditions due to agglomeration and coalescence and has only recently been demonstrated.[14]

Near ambient temperatures, many approaches have been developed to control nanocrystal size. These rely on either the use of stabilizing ligands to bind nanocrystal surfaces or the use of compartmentalized heterogeneous media, such as micellar solutions, to control growth.[30−36] These ideas have recently been extended to SCFs with general success. Water-in-sc-CO_2 microemulsions have been used as "microreactors" to produce cadmium sulfide[10] and silver[37] nanocrystals, while copper nanocrystals have been prepared in water-in-sc-ethane and water-in-propane microemulsions.[35,36] Arrested precipitation methods have also recently been used in SCFs to produce sterically stabilized silicon nanocrystals (in sc-octanol and sc-hexane) [11] and silver, platinum, and iridium nanocrystals (in sc-CO_2).[38] The key to this work has been the identification of suitable capping ligands for the SCF environment.

Here we report our finding that organic hydrocarbon capping ligands can be used to stabilize nanocrystal formation in SCW. We also find that the stabilizing ligands, in this case 1-hexanethiol, control the nanocrystal composition: copper oxide forms without ligands, while copper metal nanocrystals form in the presence of alkanethiol capping ligands. Furthermore, the processing conditions (i.e., precursor, pH, capping ligand) significantly affect the morphology and size of the nanocrystals formed in SCW, which is due to competing reaction pathways of hydrolysis and ligand exchange versus arrested growth.

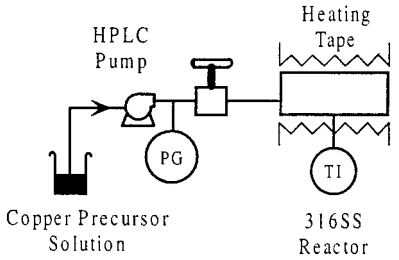

Figure 1. Schematic of the high-temperature stainless steel reactor.

Experimental Section

Nanocrystal Synthesis. Copper(II) nitrate hemipentahydrate (Aldrich), copper(II) acetate monohydrate (Acros), and 1-hexanethiol (95%, Aldrich) were used as received without further purification. The experimental apparatus consisted of a pumping system and a $^7/_8$-in.-i.d., 4-in.-long 316 stainless steel reaction cell (10 mL) described in Figure 1. For reactions without thiols, the cell was initially loaded at ambient conditions with 1.0 mL of pure water. For reactions with thiols, 900 μL of pure water with 100 μL of 1-hexanethiol was used (initial water:thiol mole ratio $\approx$ 70:1). The cell was sealed and heated to 400 °C and ~173 bar using heating tape (Barnstead/Thermolyne) and an Omega temperature controller. The cell temperature was measured with a K-type thermocouple (Omega). A 0.02 M copper precursor solution was injected into the cell via $^1/_{16}$-in.-i.d. stainless steel tubing by an HPLC pump (Beckman model 100A) at 4 mL/min until the operating pressure reached 413 bar. The solution reacts immediately upon entering the reactor, as observed visually in a separate experiment with an optical cell.[39,40] The products precipitate upon cooling the reaction. The nanocrystals were removed from the cell with either deionized water (uncapped particles) or chloroform (organic capped particles). In the case of the thiol capped nanocrystals, unreacted precursor was removed by extraction with water. The nanoparticles were filtered (Fisher, qualitative P5) to remove large agglomerates of uncapped nanocrystals and dried using a rotary evaporator (Buchi). The nanocrystals redisperse in either deionized water (uncapped particles) or chloroform (organic capped particles).

Phase Behavior of Supercritical Water and 1-Hexanethiol. The water and 1-hexanethiol phase equilibria were studied in a titanium grade 2 optical cell equipped with sapphire windows. Under the reaction conditions of 400 °C and ~413 bar (50 μL of 1-hexanethiol in 150 μL of water), water and 1-hexanethiol are miscible. This miscibility is consistent with the phase diagram for *n*-alkanes in water (*n*-pentane and *n*-heptane[41]).

Characterization Methods. Gas chromatography (GC) measurements of hexanethiol were recorded with a Hewlett-Packard 5890A gas chromatograph. Fourier transform infrared (FTIR) spectroscopy measurements were performed using a Perkin-Elmer Spectrum 2000 spectrometer with the nanoparticles dispensed on PTFE cards. Low-resolution transmission electron microscopy (TEM) images were obtained on a JEOL 200CX transmission electron microscope operating with a 120-kV accelerating voltage, while high-resolution transmission electron microscopy (HRTEM) images and selected area electron diffraction (SAED) patterns were obtained with a Gatan digital photography system on a JEOL 2010 transmission electron microscope with 1.7-Å point-to-point resolution operated with a 200-kV accelerating voltage. All samples were prepared on Electron Microscope Sciences 200-mesh carbon-coated aluminum grids by dispersing suspended nanoparticles onto the grid and evaporating the solvent. The measured

(19) Goia, D. V.; Matijevic, E. *New J. Chem.* **1998**, *22*, 1203−1215.
(20) Adschiri, T.; Kanazawa, K.; Arai, K. *J. Am. Ceram. Soc.* **1992**, *75*, 1019−1022.
(21) Adschiri, T.; Kanazawa, K.; Arai, K. *J. Am. Ceram. Soc.* **1992**, *75*, 2615−2618.
(22) Adschiri, T.; Yamane, S.; Onai, S.; Arai, K. *Proceedings of the Third International Symposium on Supercritical Fluids*, Strasbourg, France, 1994; Vol. T3, p 241.
(23) Adschiri, T.; Hakuta, Y.; Arai, K. *Ind. Eng. Chem. Res.* **2000**, *29*, 4901−4907.
(24) Matijevic, E. *J. Colloid Interface Sci.* **1987**, *117*, 593−595.
(25) Matijevic, E. *Chem. Mater.* **1993**, *5*, 412−426.
(26) McFayden, P.; Matijevic, E. *J. Colloid Interface Sci.* **1973**, *44*, 95−106.
(27) Tamura, H.; Matijevic, E. *J. Colloid. Interface Sci.* **1982**, *90*, 100−109.
(28) Hirano, M.; Etsuro, K. *J. Mater. Sci. Lett.* **1996**, *15*, 1249−1250.
(29) Hirano, M.; Etsuro, K. *J. Am. Ceram. Soc.* **1996**, *79*, 777−780.
(30) Lisiecki, I.; Pileni, M., P. *J. Am. Chem. Soc.* **1993**, *115*, 3887−3896.
(31) Lisiecki, I.; Bjoerling, M.; Motte, L.; Ninham, B.; Pileni, M., P. *Langmuir* **1995**, *11*, 2385−2392.
(32) Lisiecki, I.; Pileni, M. P. *J. Phys. Chem.* **1995**, *99*, 5077−5082.
(33) Lisiecki, I.; Billoudet, F.; Pileni, M., P. *J. Phys. Chem.* **1996**, *100*, 4160−4166.
(34) Lisiecki, I.; Filankembo, A.; Sack-Kongehl, H.; Weiss, K.; Pileni, M., P.; Urban, J. *Phys. Rev. B: Condens. Matter Mater. Phys.* **2000**, *61*, 4968−4974.
(35) Cason, J.; Roberts, C. *J. Phys. Chem. B* **2000**, *104*, 1217−1221.
(36) Cason, J. P.; Khambaswadkar, K.; Roberts, C. B. *Ind. Eng. Chem. Res.* **2000**, *39*, 4749−4755.
(37) Ji, M.; Chen, X.; Wai, C. M.; Fulton, J. L. *J. Am. Chem. Soc.* **1999**, *121*, 2631−2632.
(38) Shah, P. S.; Johnston, K. P.; Korgel, B. A. *J. Phys. Chem. B*, in press.
(39) Xiang, T.; Johnston, K. P. *J. Phys. Chem.* **1994**, *98*, 7915−7922.
(40) Xiang, T.; Johnston, K. P. *J. Solution Chem.* **1997**, *26*, 13.
(41) Connolly, J. F. *J. Chem. Eng. Data* **1966**, *11*, 13.

Table 1. Nanocrystal Formation in Supercritical Water[a]

	starting material	conc (mM)	temp (°C)	init pressure (bar)[b]	capping ligand	pH at room temp	average diameter (nm)	distribution (nm)	product
A	$Cu(NO_3)_2$	20	400	200		3.40	16.7	8−35	CuO
B	$Cu(CH_3COO)_2$	20	400	200		5.25	30.9	10−97	Cu, Cu_2O
C	$Cu(NO_3)_2$	20	400	200	C_6SH	3.40	7.0	3−15	Cu
D	$Cu(NO_3)_2$	20	425	220	C_6SH	3.40	7.8	4−14	Cu
E	$Cu(NO_3)_2$	20	450	240	C_6SH	3.40	9.2	4−15	Cu
F	$Cu(CH_3COO)_2$	20	400	200	C_6SH	5.25	33.8	10−89	Cu, Cu_2O
G	$Cu(CH_3COO)_2$	20	400	200	$C_{12}SH$	5.25	26.5	10−68	Cu, Cu_2O
H	$Cu(NO_3)_2$	2	400	200	C_6SH	4.59	40.8	12−111	
I	$Cu(NO_3)_2$ [c]		400	200	C_6SH		36.1	9−80	
J	$Cu(NO_3)_2$ + NaOH	20	400	200	C_6SH	6.00	45.0	13−187	
K	$Cu(CH_3COO)_2$ + HNO_3	20	400	200	C_6SH	2.66	47.4	11−133	

[a] All reactions were performed with 900 μL of pure water and 100 μL of thiol unless otherwise noted. [b] Based on PVT data for pure water. [c] Copper nitrate (0.02-M) and 1-hexanethiol were mixed before heating and pressurizing. A reaction occurred immediately resulting in the formation of a yellow solid.

Table 2. Growth Analysis of Nanocrystal Formation in Supercritical Water

	product	predominant structure	agglomeration	average diameter (nm)	distribution moment μ_1	distribution moment μ_3	growth mechanism
A	CuO	icosahedral	moderate	16.7	1.23	0.90	diffusion
B	Cu, Cu_2O	octahedral	high	30.9	1.75	0.76	coagulation
C	Cu	icosahedral	low	7.0	1.19	0.92	diffusion
D	Cu	icosahedral	low	7.8	1.08	0.96	diffusion
E	Cu	icosahedral	low	9.2	1.14	0.94	diffusion
F	Cu, Cu_2O	octahedral	high	33.8	1.40	0.84	coagulation
G	Cu, Cu_2O	octahedral	high	26.5	1.27	0.88	coagulation
H		mixture	moderate	40.8	1.44	0.83	coagulation
I		ellipsoidal	low	36.1	1.40	0.86	coagulation
J		mixture	moderate	45.0	1.67	0.75	coagulation
K		mixture	high	47.4	1.38	0.86	coagulation

lattice separations were indexed against standards[42] for copper, Cu_2O, and CuO. UV−visible absorbance spectroscopy was performed using a Varian Cary 300 UV−visible spectrophotometer with the capped nanoparticles dispersed in chloroform. X-ray photoelectron spectroscopy (XPS) was performed on a Physical Electronics XPS 5700, with a monochromatic Al X-ray source (Kα excitation at 1486.6 eV). For XPS, the samples were deposited on a silicon wafer (cleaned with a 50:50 mixture of methanol/HCl), vacuum-dried at 25 °C to remove all residual solvent, and stored under nitrogen.

Results

The nanocrystals synthesized in SCW were characterized using several techniques, including TEM, XPS, EDS, and SAED. Several factors, including precursor concentration, solution pH, capping ligand, and the type of precursor, affect the crystal structure, size, morphology, and degree of agglomeration of the nanocrystals. Tables 1 and 2 summarize all results.

Copper and Copper Oxide Particle Formation in Supercritical Water (no Capping Ligands). Figure 2 shows TEM images of size-polydisperse particles formed using $Cu(NO_3)_2$. Particle diameters range from 8 to 35 nm with an average diameter of 16.7 nm. HRTEM (Figure 2a) reveals relatively spherical and crystalline particles. Although some individual particles can be seen on the TEM grid after deposition (Figure 2b), a significant amount of aggregation has occurred (Figure 2c). SAED revealed that the particle cores are tenorite CuO.[43] The lattice spacing in the HRTEM images (such as those in Figure 2a) of 2.53 Å are also consistent with the bulk value of

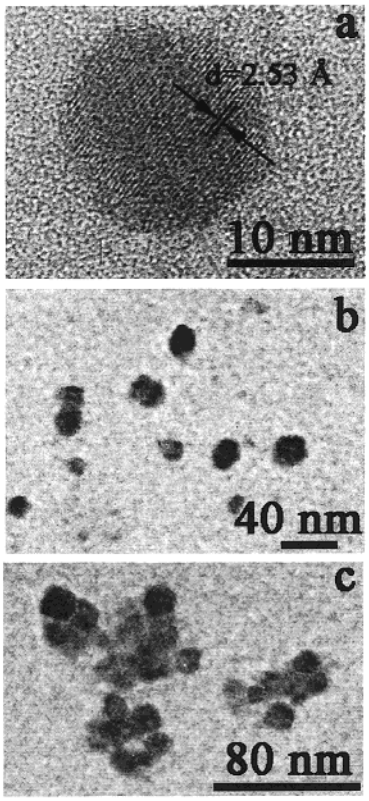

Figure 2. (a) High-resolution and (b, c) low-resolution TEM images of CuO nanoparticles synthesized via $Cu(NO_3)_2$ in SCW without capping ligands.

(42) Urban, J.; Sack-Kongehl, H.; Weiss, K. *Catal. Lett.* **1997**, *49*, 101−108.

(43) Figure contained within Supporting Information.

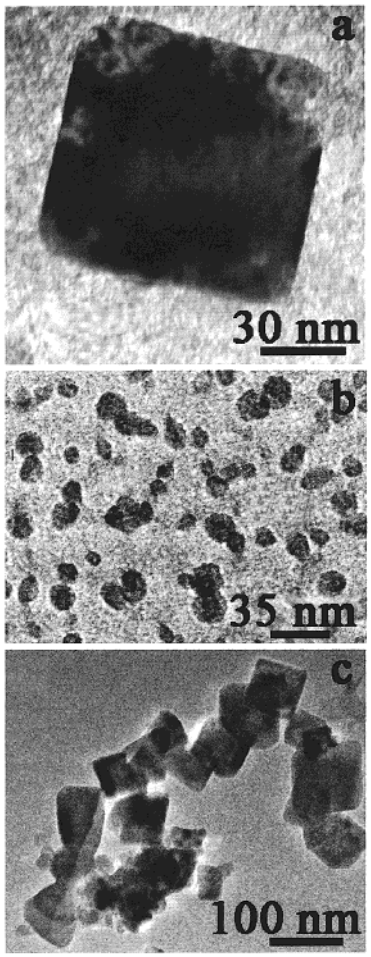

Figure 3. (a) High-resolution and (b) low-resolution TEM images of slightly agglomerated, uncapped Cu_2O or elemental copper nanoparticles and (c) TEM images of highly agglomerated, uncapped Cu_2O or elemental copper nanoparticles synthesized via $Cu(CH_3COO)_2$ in SCW. Note in (a) and (c) the appearance of different morphologies than in Figure 2.

2.51 Å for the ⟨002⟩ or ⟨−111⟩ lattice spacing in tenorite CuO. XPS, shown in Figure 6a, further confirmed that particles formed using $Cu(NO_3)_2$ without thiol were composed of CuO: the Cu 2p core level binding energy of 933.7 eV is characteristic of Cu^{II} cations, and the satellite or shake-up regions for Cu^{2+} at 945 and 965 eV [44] result from electron transfer to the core hole to yield d^9 character.[45] All of these techniques indicate $Cu(NO_3)_2$ degradation in SCW yields CuO particles.

When $Cu(CH_3COO)_2$ is used as the precursor, particles form with a larger average diameter of 30.9 nm and a broader distribution ranging from 10 to 97 nm (Figure 3) than those formed using $Cu(NO_3)_2$. The particles exhibit an octahedral morphology (projected as cubic in Figure 3a or as hexagonal in Figure 3c) and a greater tendency to agglomerate (Figure 3b and c). SAED[43] shows that the particles contain Cu cores. Many HRTEM images of the $Cu(CH_3COO)_2$ system (such as Figure 5a), however, reveal both Cu_2O (3.07 Å compared to 3.02 Å for the ⟨110⟩ lattice spacing) as well as copper metal nanocrystals. XPS in Figure 6 show Cu 2p core level binding energy characteristic of elemental copper or Cu_2O. Unfortunately, from XPS data alone, it is difficult to distinguish the copper oxidation state between Cu^0 and Cu^I due to the effects of crystal size and surface coverage on the binding energy.[46] However, it appears that $Cu(CH_3COO)_2$ degradation in SCW yields a mixture of Cu and Cu_2O particles.

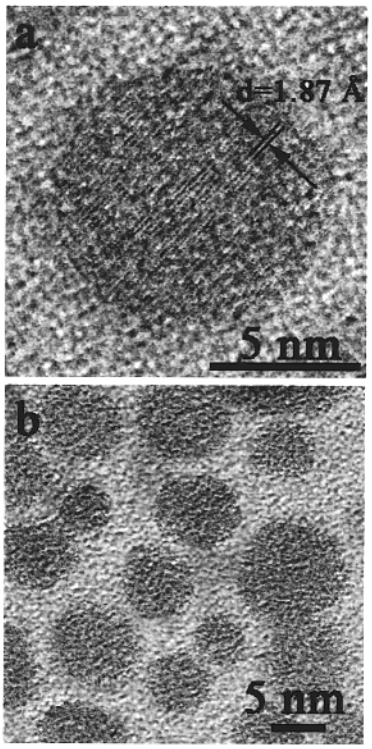

Figure 4. (a) High-resolution and (b) low-resolution TEM images of 1-hexanethiol stabilized copper nanoparticles synthesized via $Cu(NO_3)_2$ in SCW. Note that the nanoparticles are stabilized and not agglomerated despite the close proximity.

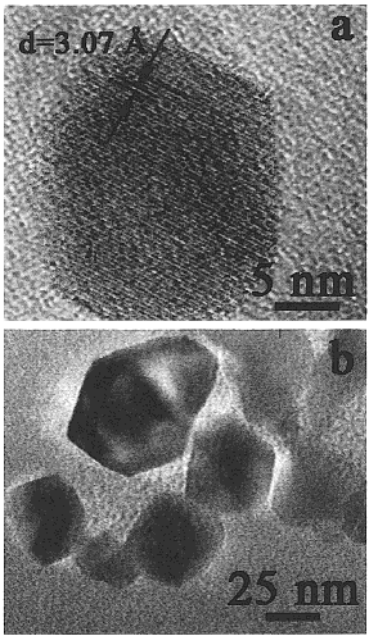

Figure 5. (a) High-resolution and (b) low-resolution TEM images of 1-hexanethiol stabilized copper nanoparticles synthesized via $Cu(CH_3COO)_2$ in SCW. Note that the particles are not stabilized and highly agglomerated despite being passivated with a capping ligand.

Formation of Ligand-Stabilized Copper Nanocrystals in Supercritical Water. 1-Hexanethiol was added to the reactor

(44) Chusuei, C. C.; Brookshier, M. A.; Goodman, D. W. *Langmuir* **1999**, *15*, 2806−2808.

(45) Borgohain, K.; Singh, J., B.; Rama Rao, M., V.; Shripathi, T.; Mahamuni, S. *Phys. Rev. B: Condens. Matter Mater. Phys.* **2000**, *61*, 11093−11096.

(46) Carley, A. F.; Dollard, L. A.; Norman, P. R.; Pottage, C.; Roberts, M. W. *J. Electron Spectrosc.* **1999**, *98*−*99*, 223−233.

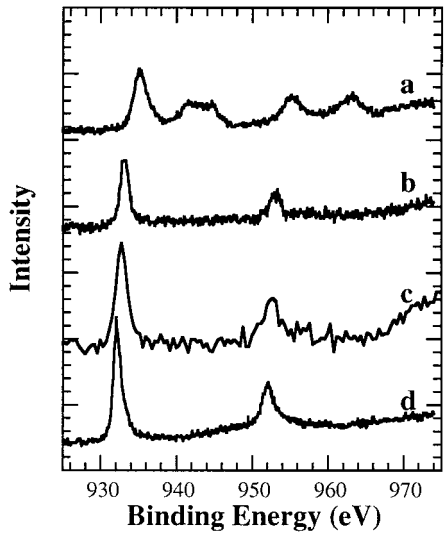

Figure 6. XPS of uncapped particles produced via (a) $Cu(NO_3)_2$ and (b) $Cu(CH_3COO)_2$ and XPS scan of organically capped nanoparticles produced with (c) $Cu(NO_3)_2$ and (d) $Cu(CH_3COO)_2$. All scans are offset for clarity. Cu 2p core level binding energy for copper(II) at 934 eV and copper(0) at 932 eV.

as a capping ligand to control particle growth in SCW. Although alkanethiols do not dissolve in water at room temperature, 1-hexanethiol dissolves in supercritical water at the concentrations studied (see above).[41] GC analysis of water/1-hexanethiol mixtures confirmed that the organic capping ligands were stable in SCW under the reaction conditions explored. For residence times up to 30 min, 1-hexanethiol did not decompose. After 45 min, decomposition product concentrations could be detected on the order of 10−100 times smaller than the initial 1-hexanethiol concentration.

Nanocrystals formed using $Cu(NO_3)_2$ in the presence of 1-hexanethiol with a starting solution pH of 3.4 have an average diameter of 7.0 nm with crystalline cores and spherical shape, as shown in Figure 4. The nanocrystal surfaces rarely touch in the TEM image due to the bulky capping ligand layer surrounding each particle (Figure 4b). The average size and the size distribution (3−15 nm) of these nanoparticles are smaller than those of the uncapped particles (16.7 nm) by a factor of more than 2. SAED of the nanocrystals[43] show that the nanocrystal cores are composed of elemental Cu. The HRTEM images, such as Figure 4a, reveal d spacings of 1.87 Å (compared to 1.81 Å for the ⟨200⟩ lattice spacing) characteristic of copper. Furthermore, the Cu 2p core level binding energies consistent with elemental copper appear in the XPS data.[46] The spherical nanocrystal shape is consistent with icosahedra formation, which is well known for copper nanocrystals smaller than ∼7 nm.[47−49] Room-temperature UV−visible absorbance spectra in Figure 7 are characteristic of Cu nanocrystals,[32,33] as the surface plasmon resonance for bulk copper metal (2.15 (560 nm) to 2.2 eV (580 nm)) is noticeably absent. On the basis of Mie theory, the surface plasmon resonance for copper nanocrystals is expected to have strong broadening for particles smaller than 100 Å.[33] Increasing the reaction temperature to 425 and 450 °C resulted in an increase in the average particle diameter (7.8 and 9.2 nm, respectively).

TEM images of copper nanocrystals formed with $Cu(CH_3COO)_2$ precursor in the presence of 1-hexanethiol at a starting solution pH of 5.25 under pressure, temperature, and concentration conditions identical to the nitrate system above, are shown in Figure 5. The addition of the capping ligand has little effect on the average size (33.8 nm), size distribution, morphology, and oxidation state of the particles. Despite the apparent lack of an effect on size and morphology, the ligands are nonetheless bound to the particle surface. FTIR spectra[43] show the characteristic methyl and methylene stretches of the capping ligands after removal of all unbound ligands from the sample; however, these capping ligands apparently do not effectively prevent agglomeration or quench growth. A longer capping ligand (1-dodecanethiol) helped stabilize a small amount of particles (not shown), but most of the particles agglomerated as with 1-hexanethiol.

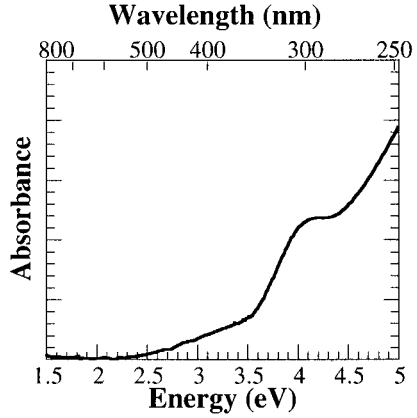

Figure 7. Room-temperature UV−visible spectra of organically capped copper nanoparticles synthesized via $Cu(NO_3)_2$ and 1-hexanethiol.

Since the reaction mechanism may involve hydrated and hydroxylated complexes, pH differences could be the source of the significant variations in particle formation using the acetate and nitrate precursors. For example, Baes and Mesmer[50] have shown at room temperature that Cu^{II} exists as hydrated Cu^{2+} at acidic conditions and as $Cu_2(OH)_2^{2+}$ under basic conditions (pH >4). Differences in hydration could be present at higher temperatures, although they have not been studied. Particles formed using $Cu(NO_3)_2$ after raising the pH to 6.0 with NaOH appeared very similar to those produced with $Cu(CH_3COO)_2$ at a pH of 5.25, with 45.0-nm average particle diameter and size distribution of 13−187 nm. Cu nanocrystals synthesized using 2 mM $Cu(NO_3)_2$ with a starting pH of 4.59 were also large (40.8 nm) with a broad size distribution. Experiments using $Cu(CH_3COO)_2$ after the pH was lowered to 2.66 with HNO_3, however, yielded large agglomerated particles with an average particle diameter of 47.4 nm and a size distribution of 11−133 nm. Therefore, both pH and the nature of the anions affects nanocrystal formation.

It is worth noting that mixing $Cu(NO_3)_2$ and 1-hexanethiol at room temperature produced a yellow precipitate likely due to the formation of a copper−thiol complex. When heated to 400 °C and ∼413 bar, this mixture produced large spherical or ellipsoidal size-polydisperse particles 36.1 nm in diameter ranging 9−80 nm.[43] The particles exhibit little aggregation on the TEM grid with unique morphologies compared to the synthesis with $Cu(CH_3COO)_2$.

Growth Analysis of Particle Formation. After nucleation, the particles may grow either by condensation (diffusion-limited growth) or by fusion of the metal cores (coagulation).[38,51−53] Analysis of the moments of the size distribution provides insight

(47) Olynick, D. L.; Gibson, J. M.; Averback, R. S. *Appl. Phys. Lett.* **1996**, *68*, 343−345.
(48) Gillet, M. *Surf. Sci.* **1977**, *67*, 139−157.
(49) Urban, J.; Sack-Kongehl, H.; Weiss, K. *Z. Phys. D* **1996**, *36*, 73−83.
(50) Baes, C. F., Jr.; Mesmer, R. E. *The Hydrolysis of Cations*; Wiley: New York, 1976.

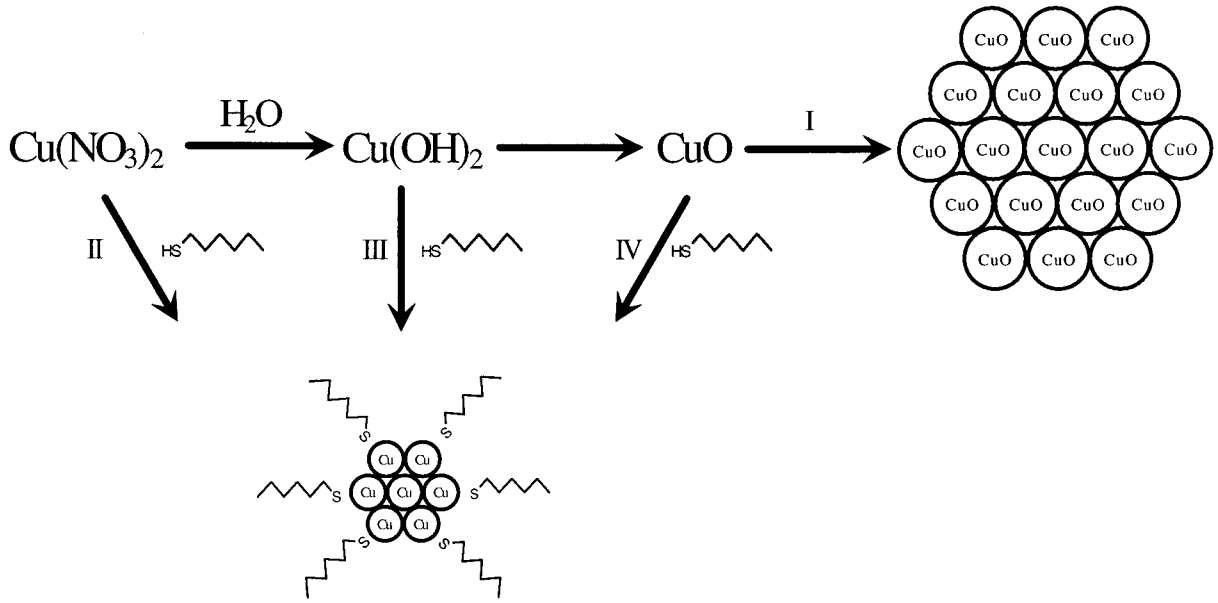

Figure 8. Proposed schematic representation of reaction mechanism for the formation of organically capped copper nanoparticles in supercritical water via $Cu(NO_3)_2$.

into the growth mechanism. The first moment, $\mu_1 = r_3/r_h$, and the third moment, $\mu_3 = r_1/r_3$, describe the polydispersity of the sample. The moments are functions of the arithmetic mean radius $r_1 = \sum r_i/N_\infty$, the cube-mean radius $r_3 = \sqrt[3]{(\sum r_i^3/N_\infty)}$, and the harmonic mean radius $r_h = N_\infty/\sum 1/r_i$, where N_∞ is the total number of particles in the sample. Values of $\mu_1 > 1.25$ and $\mu_3 < 0.905$ indicate that growth occurs by coagulation, whereas diffusion-limited growth occurs when μ_1 and μ_3 approach unity.[38,51−53] In the case of the experiments with $Cu(NO_3)_2$ at pH ∼3, μ_1 and μ_3 approach unity (Tables 1 and 2 summarize the size distribution analysis of all the experiments), which suggests that growth occurs through a diffusion-limited mechanism of Cu atom diffusion to nucleated particles. In nearly all other experiments, growth occurs primarily through coagulation of metal cores and broad size distributions result.

Discussion

The precursors, $Cu(NO_3)_2$ and $Cu(CH_3COO)_2$, produce qualitatively different nanocrystals. Without alkanethiol, the nitrate precursor yields spherical CuO particles ∼17 nm in diameter. The acetate precursor gives 30−40-nm-diameter octahedral particles with mixed Cu and Cu_2O composition. In the presence of alkanethiol, $Cu(NO_3)_2$ gives 7-nm-diameter spherical Cu nanocrystals; whereas, there is little change in the nanocrystal size and shape when $Cu(CH_3COO)_2$ is used. Below, we describe the mechanistic factors that lead to these differences. The mechanism can be viewed as a competition between hydrolysis to large oxidized copper particles versus ligand exchange and arrested growth by thiols to produce small monodisperse nanoparticles.

Recently, Fulton et al.[54] used X-ray absorption fine structure (XAFS) to determine that ion-pairing and hydrolysis mechanisms for Cu^I and Cu^{II} in SCW are temperature dependent:

$$[Cu(H_2O)_6]^{2+} + m(NO_3^-) \xrightarrow{350\ ^\circ C > T > 100\ ^\circ C} [Cu(H_2O)_{6-m}(NO_3^-)_m]^{2-m} + mH_2O \quad (1)$$

$$[Cu(H_2O)_6]^{2+} + m(NO_3^-) \xrightarrow{T > 400\ ^\circ C} CuO + 2H^+ + 5H_2O + m(NO_3^-) \quad (2)$$

Above 400 °C, hydrolysis results in CuO formation. Adschiri et al. have also described metal oxide formation in SCW using metal nitrates[55] as a two-step hydrolysis and dehydration reaction.[20,21] On the basis of these studies, copper nitrate hydrolysis, in the absence of alkanethiol, may be described by pathway I in Figure 8, which leads to nucleation of the oxide, CuO.

In the presence of 1-hexanethiol, ligand exchange of thiol for anions and thiol-induced Cu^{II} reduction can lead to Cu particles by pathways II, III, and possibly IV shown in Figure 8. Pathways II and III compete with the hydrolysis/dehydration pathway. This mechanism is consistent with the observed effects of anion, pH, and thiol ligand on particle size, size distribution, and oxidation state as discussed below.

Ligand Effects. When alkanethiol is added to the $Cu(NO_3)_2$ solutions during nanocrystal formation, Cu nanocrystals result in lieu of CuO. Although the nitrate ion serves as an oxidizing agent in SCW[55] to favor CuO, the thiol participates in Cu^{II} reduction to Cu^0 during nanocrystal formation through either reaction pathway II, III, or IV in Figure 8. The steric stabilization provided by alkanethiol results in diameters half the size of those produced without capping ligands.

Previous investigators have shown that, during the self-assembly of alkanethiol monolayers on monolithic CuO surfaces, the alkanethiol reduces the oxide surface to copper metal before binding through the following mechanism:[56,57]

(51) Friedlander, S. K.; Wang, C. S. *J. Colloid Interface Sci.* **1966**, *22*, 126−132.
(52) Pich, J.; Friedlander, S. K.; Lai, F. S. *Aerosol Sci.* **1970**, *1*, 115−126.
(53) Swift, D. L.; Friedlander, S. K. *J. Colloid Interface Sci.* **1964**, *19*, 621−647.
(54) Fulton, J. L.; Hoffman, M. M.; Darab, J. G.; Palmer, B. J.; Stern, E. A. *J. Phys. Chem. A* **2000**, *104*, 11651−11663.
(55) Nitrates are strong oxidants in SCW: (a) Chlistunoff, J.; Ziegler, K. J.; Lasdon, L.; Johnston, K. P. *J. Phys. Chem. A* **1999**, *103*, 1678−1688. (b) Ziegler, K. J., Chlistunoff, J., Lasdon, L., Johnston, K. P. *Comput. Chem.* **1999**, *23*, 421−434.
(56) Ron, H.; Cohen, H.; Matlis, S.; Rappaport, M.; Rubinstein, I. *J. Phys. Chem.* **1998**, *102*, 9861−9869.
(57) Sung, M. M.; Sung, K.; Kim, C. G.; Lee, S. S.; Kim, Y. *J. Phys. Chem. B* **2000**, *104*, 2273−2277.

$$2HSC_xH_{2x+1} + CuO \rightarrow (SC_xH_{2x+1})_2 + Cu + H_2O \quad (3)$$

$$HSC_xH_{2x+1} + Cu \rightarrow C_xH_{2x+1}SCu + {}^1/_2H_2 \quad (4)$$

If CuO particles, which are highly insoluble in SCW, nucleated and grew via reaction pathway I, the thiol would have limited ability to reduce the CuO in the cores of the growing nanocrystals. Cu nanocrystals may be produced through pathway IV only if reduction occurs before significant growth of CuO crystals takes place. Because the nanocrystals formed from $Cu(NO_3)_2$ in the presence of thiol exhibit Cu crystalline cores with few lattice defects (as confirmed by HRTEM and XPS), it is unlikely that these cores came from previously grown CuO nuclei or small nanocrystals. Furthermore, the Cu nanocrystal size distributions in experiments C−E are consistent with diffusion-limited growth by copper atom addition to growing Cu nanocrystals rather than the aggregation of uncapped CuO particles. Therefore, Cu^{II} reduction likely occurs prior to nanocrystal growth via pathway II or III.

In subcritical studies, alkanethiol has been found to reduce Cu_2O to elemental copper through the reaction mechanism[56,57]

$$2HSC_xH_{2x+1} + Cu_2O \rightarrow 2C_xH_{2x+1}SCu + H_2O \quad (5)$$

The alkanethiol, however, does not appear to readily aid the reduction of Cu_2O to elemental copper when $Cu(CH_3COO)_2$ is used as the precursor for nanocrystal growth in SCW. In addition, thiol does not appear to affect the size or morphology of the nanocrystals. Nevertheless, FTIR spectra show that the thiol binds to the particle surface to stabilize the particles in organic solutions, whereas, uncapped particles precipitate within minutes. It appears that the thiol binding rate cannot compete with the particle growth rate when $Cu(CH_3COO)_2$ is used as the precursor.

pH and Anion Effects. In the absence of thiol, $Cu(CH_3COO)_2$ produces particles that consist of a mixture of copper metal and Cu_2O, in contrast with CuO particles produced using $Cu(NO_3)_2$. These results are consistent with Darr and Poliakoff,[8] who showed that the hydrolysis of metal−organic complexes, in contrast with metal salts, produces reduced metal oxides or metal particles. Complexes of coinage metals, such as copper, are particularly susceptible to reduction.[8]

A key difference between the $Cu(NO_3)_2$ and $Cu(CH_3COO)_2$ solutions is the pH prior to nanocrystal formation. Although the pH is unknown for these systems in SCW, the relative pH may follow approximate trends at ambient conditions, based on previous in situ measurements for related systems.[39,40] In subcritical water, the Pourbaix diagram indicates that Cu is favored at low pH and oxidized copper species at higher pH due to reactions with OH ligands.[58] Our results are consistent with this trend in that Cu alone is formed only in the $Cu(NO_3)_2$ experiments with thiol at low pH and oxidized species are present at higher pH values. For example, when NaOH was added to raise the pH to 6.0, ∼45-nm-diameter octahedral Cu and Cu_2O nanocrystals were produced. Here, the thiol was less effective in reducing the copper and stabilizing the particles. Both of these trends would be consistent with greater selectivity toward hydrolysis, due to an increase in pH, relative to pathway II.

The effects of pH and anion structure are further described in the experiment where HNO_3 was added to $Cu(CH_3COO)_2$. Despite having a pH similar to those in experiments with $Cu(NO_3)_2$ only, which yielded small nanocrystals, these crystals were quite large (47 nm in diameter) and included Cu_2O. Clearly, these changes are not due to pH alone. Thus, it is likely that the complexation of acetate anion to copper inhibits ligand exchange reactions with thiol and the ability of thiol to reduce and stabilize the growing particles, relative to the case of the nitrate ion. The possibility of a copper(II) acetate dimer, which is known to be stable at ambient temperature, could also influence the hydrolysis and ligand capping reaction pathways.

Conclusions

Organic alkanethiol capping ligands can be used successfully to stabilize Cu nanocrystal formation in supercritical water. The formation of the organically capped nanocrystals occurs in a miscible mixture of organic thiols and water at supercritical conditions. Despite the highly destructive environment of supercritical water, the alkanethiol was relatively stable for the length of the reaction. Competitive pathways are present between hydrolysis to large polydisperse oxidized particles and ligand exchange and arrested growth favoring smaller Cu nanocrystals. $Cu(NO_3)_2$ was found to be a suitable precursor to produce 7-nm-diameter Cu nanocrystals at low starting pH with alkanethiol. Higher pH increased particle sizes and led to Cu_2O along with Cu. The alkanethiol plays a key role in stabilization and quenching particle growth. The alkanethiol also controls the oxidation state of the nanocrystals by reducing Cu^{II} to Cu^0; in the absence of thiol, the nitrate precursor yields CuO particles. When $Cu(CH_3COO)_2$, was used as a precursor with or without alkanethiol, large particles, 10−30 nm in diameter, were produced with a mixture of Cu and Cu_2O. In the proposed mechanism for nanocrystal synthesis, larger more oxidized particles are produced via a hydrolysis route, which are favored by higher pH, and less effective early ligand exchange by thiol. The $Cu(NO_3)_2$ precursor at low pH favors early thiol ligand exchange and arrested growth, which competes with hydrolysis. Analyses of the moments of the particle size distributions further support a competitive mechanism between hydrolysis to large polydisperse oxidized particles favored by aggregation and arrested growth of low polydispersity Cu particles smaller than 10 nm by diffusion-limited growth.

Acknowledgment. We thank John Mendenhall for assistance with TEM imaging, Stephen Swinnea for assistance with electron diffraction analysis, and Jose Lozano for assistance with XPS. We thank the Department of Energy, National Science Foundation, Dupont, the Welch Foundation, and ACS for support.

Supporting Information Available: Figures showing FTIR of alkanethiol capped particles, SAED patterns, and TEM images of particles produced via the copper−thiol complex. This material is available free of charge via the Internet at http://pubs.acs.org.

JA010824W

(58) Beverskog, B.; Puigdomenech, I. *J. Electrochem. Soc.* **1997**, *144*, 3476−3483.